

# Autonomous Retroflexion of a Magnetic Flexible Endoscope

Piotr R. Slawinski, *Student Member, IEEE*, Addisu Z. Taddese, *Student Member, IEEE*, Kyle B. Musto, Keith L. Obstein, and Pietro Valdastri, *Senior Member, IEEE*

**Abstract**—Retroflexion during colonoscopy is typically only practiced in the wider proximal and distal ends of the large intestine owing to the stiff nature of the colonoscope. This inability to examine the proximal side of the majority of colon folds contributes to today’s suboptimal colorectal cancer detection rates. We have developed an algorithm for autonomous retroflexion of a flexible endoscope that is actuated magnetically from the tip. The magnetic wrench applied on the tip of the endoscope is optimized in real time with data from pose detection to compute motions of the actuating magnet. This is the first example of a completely autonomous maneuver by a magnetic endoscope for exploration of the gastrointestinal tract. The proposed approach was validated in plastic tubes of various diameters with a success rate of 98.8% for separation distances up to 50 mm. Additionally, a set of trials was conducted in an excised porcine colon observing a success rate of 100% with a mean time of 19.7 s. In terms of clinical safety, the maximum stress that is applied on the colon wall with our methodology is an order of magnitude below what would damage tissue.

**Index Terms**—Flexible robots, medical robots and systems, motion control, surgical robotics: steerable catheters/needles.

## I. INTRODUCTION

**C**OLONOSCOPY is the gold standard screening method for colorectal cancer; the second and third most common

Manuscript received September 9, 2016; accepted January 23, 2017. Date of publication February 13, 2017; date of current version March 10, 2017. This letter was recommended for publication by Associate Editor I. I. Iordachita and Editor K. Masamune upon evaluation of the reviewers comments. This work was supported in part by the National Institute of Biomedical Imaging and Bioengineering, USA, of the National Institutes of Health under award R01EB018992, in part by the National Science Foundation, USA, under Grants CNS-1239355 and IIS-1453129, in part by the National Science Foundation Graduate Research Fellowship Program under Grant 1445197, and in part by the Royal Society, U.K.

P. R. Slawinski, A. Z. Taddese, and K. B. Musto are with the Science and Technology of Robotics in Medicine Laboratory, Department of Mechanical Engineering, Vanderbilt University, Nashville, TN 37235 USA (e-mail: piotr.r.slawinski@vanderbilt.edu; addisu.z.taddese@vanderbilt.edu; kyle.b.musto@vanderbilt.edu).

K. L. Obstein is with the Division of Gastroenterology, Hepatology, and Nutrition, Vanderbilt University Medical Center, Nashville, TN 37235 USA, and also with the Science and Technology of Robotics in Medicine Laboratory, Department of Mechanical Engineering, Vanderbilt University, Nashville, TN 37235 USA (e-mail: keith.obstein@vanderbilt.edu).

P. Valdastri is with the Institute of Robotics, Autonomous Systems and Sensing, School of Electronic and Electrical Engineering, University of Leeds, Leeds LS2 9JT U.K., and also with the Science and Technology of Robotics in Medicine Laboratory, Department of Mechanical Engineering, Vanderbilt University, Nashville, TN 37235 USA (e-mail: p.valdastri@leeds.ac.uk).

This paper has supplementary downloadable material available at <http://ieeexplore.ieee.org>.

Color versions of one or more of the figures in this paper are available online at <http://ieeexplore.ieee.org>.

Digital Object Identifier 10.1109/LRA.2017.2668459

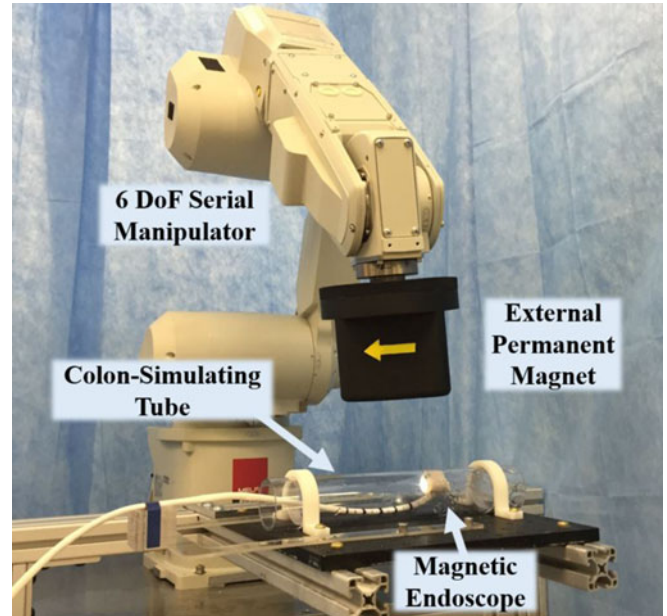


Fig. 1. Magnetic colonoscopy platform.

form of cancer worldwide for females and males, respectively [1]. Adenoma, or benign tumor, detection rate (ADR) during colonoscopy has been shown to be a predictor of the risk of cancer developed between routine screenings [2]. Although ADRs are over 25% for men and 15% for women, most experts agree that these can be improved. A 1% increase in ADR has also been shown to coincide with a 3% decrease in the risk of cancer [3]. Although the use of the flexible endoscope has been the standard diagnostic tool for over 50 years, adenoma miss rates of 15 to 41% have been reported [3], [4]. These low performance rates are hypothesized to result from polyp positioning on the proximal side of folds and flexures [4]. Retroflexion is a maneuver where the endoscope is rotated backwards inside a lumen for an improved endoscopic view behind folds and, owing to the stiff nature of the traditional endoscope, is typically only practiced in the proximal and distal ends of the colon where the lumen diameter is largest. The maneuver is recommended by the American Society of Gastrointestinal Endoscopy and labeled as an “essential” element of colonoscopy [5]. Additionally, past studies have shown that retroflexion cannot be replaced by extensive endoscopy manipulation since it is inadequate for viewing behind folds [6].

As emphasized in literature, the use of push-actuated flexible endoscopes increases the chance of tissue damage and often results in colon wall deformation and looping, which account for 90% of pain during colonoscopy procedures [7]. This has motivated the development of several forward-driving endoscope modalities, of which tethered magnetic actuation has been labeled as most feasible [8], [9].

Retroflexion using a tethered magnetically actuated capsule was demonstrated in previous work using open-loop teleoperation [10]; however, the lack of position and orientation feedback of the device resulted in a steep learning curve and long procedure duration. Developing an autonomous retroflexion maneuver is crucial to the procedure to reduce adenoma miss rate. It is worth mentioning that, owing to the convoluted geometry and deformable nature of the colon, it is impractical to pursue development of an automated system—one where rules are defined and fixed in advance—but rather an autonomous one, where a system’s behavior is constrained by a set of rules [11], but can adapt to a dynamic environment as necessary. Thus, decisions on the motion of the tip of the endoscope should be made algorithmically in real-time, eliminating any teleoperative input from the user for the specific task of retroflexion. Additionally, an autonomous system reduces the level of experience required to perform the maneuver, thus maintaining the focus on diagnostics during retroflexion training rather than endoscope maneuverability. Crucial to this aim are real-time localization and closed loop control of the tip of the endoscope, both demonstrated previously by our group [12]–[15] and others [16]–[18].

In this letter, we present an algorithm for retroflexing a magnetic endoscope on experimental setups of increasing complexity. Using real-time magnetic localization [12], the tip of the endoscope, starting from a straight alignment with the lower-bowel lumen, is retroflexed by a magnetic wrench applied from an external permanent magnet (EPM) that is attached to a 6 degree-of-freedom (DoF) industrial manipulator as seen in Fig. 1. The algorithm, running at a rate of 65 Hz (real time), optimizes the magnetic wrench that is applied on the device’s tip so as to drive the endoscope toward a target pose, as a function of end-effector motion.

The contribution of this work is the optimization of the end-effector motion in task space making it more suitable for applications where task-space constraints (*e.g.* avoiding collision with the patient’s body) exist. Further, in our previous work [13], [15], the error term for the closed-loop orientation controller was defined by the cross product of the current and desired heading vectors. While this error term describes the shortest angular path between the heading vectors, it is not necessarily the most efficient for magnetic manipulation. In this work, we demonstrate that a more efficient error term can be found, especially in the context of retroflexion.

This letter contains a brief system description, detailed discussion of the algorithm used, bench-top results showing the success rate and time to retroflex in tubes of various diameters as well as varied end effector heights from the top of the lumen, and results of an *ex vivo* trial on a porcine lumen. As with development of any medical device, of utmost importance is patient safety. In addition to algorithm validation, we developed

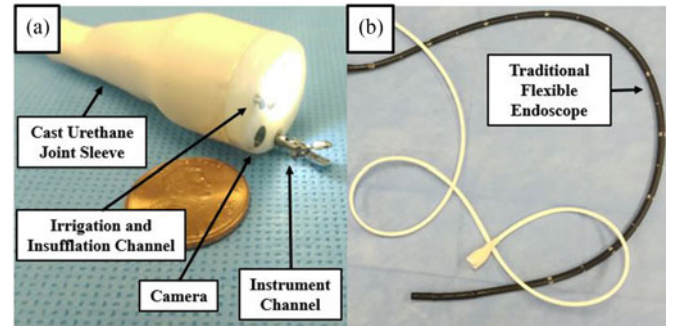


Fig. 2. a) The tip of the magnetically actuated endoscope (white) maintains all functionality of a traditional endoscope b) while having a more compliant body.

an experimental platform to estimate the maximal stress that is applied onto the lumen during our retroflexion maneuver.

## II. PLATFORM DESCRIPTION

The system consists of an endoscope with a magnet-embedded tip and serial 6 DoF manipulator. The manipulator (RV-6SDL, Mitsubishi Corp, Japan) carries a cylindrical external permanent magnet (EPM) (N52, 4” diameter and length, axial magnetization with residual flux density of 1.48 T, ND\_N-10195, Magnet World Inc., USA) at its end effector. The endoscope’s tip, shown in Fig. 2(a), is fabricated from 3D printed material (VeroWhitePlus RGD835, Stratasys Ltd., MN, USA) and has a diameter and length of 20.6 mm and 18.1 mm, respectively. A flexible sleeve (Cast Urethane - Elastomer 25A) joins the tip with a 6.5 mm diameter endoscope body (Pebax 35D Propell), Fig. 2(b), through which electrical wires as well as a tool and an irrigation channel are routed. The tip contains a flexible circuit with localization sensors as well as an embedded permanent magnet (EM) (D77-N52, 7/16” diameter and length, axial magnetization with residual flux density of 1.48 T, K&J Magnetics Inc, USA).

## III. THEORETICAL APPROACH

The theoretical formulations used are based on the work of Mahoney and Abbott who demonstrated closed-loop control of a dipole-driven wireless capsule [18]. The linearizations of magnetic force and torque that the EPM exerts onto the capsule, or in our case onto the tip of the endoscope, have been analytically derived and explicitly presented in our previous work [13]. Hereafter, bold letters indicate vectors ( $\mathbf{v}$ ), a dot above a letter indicates a time derivative ( $\dot{\mathbf{v}}$ ), a hat over a bold letter indicates a unit vector ( $\hat{\mathbf{v}}$ ), and an uppercase letter indicates a matrix ( $M$ ).  $I$  denotes the identity matrix. We attempt to maintain the same nomenclature as these previous works for clarity and define the magnetic moment direction vectors of the EM and EPM as  $\hat{\mathbf{m}}_c$  and  $\hat{\mathbf{m}}_a$ , respectively. The EM is aligned such that  $\hat{\mathbf{m}}_c$  corresponds to the heading of the device and thus points to the outside of the tip while aligned with its central axis. All vectors are expressed in the world (base of manipulator) frame with  $\mathbf{p} = \mathbf{p}_c - \mathbf{p}_a$  indicating the relative position vector of the endoscope from the actuating magnet.

This work is centered around the task of continuously applying a magnetic wrench onto the EM, which we assume to be in quasistatic equilibrium with the rest of the body of the flexible endoscope, such that the tip is reversed by 180° from its heading  $\hat{\mathbf{m}}_c$  at the start of the maneuver to a final heading  $\hat{\mathbf{m}}_{c_{des}}$ . In the first subsection, we describe the algorithm which consists of solving a constrained optimization problem. In the second subsection, we discuss the reasoning behind the optimal solutions that are computed.

### A. Optimizing External Permanent Magnet Motion

In this algorithm, we continuously maximize the infinitesimal magnetic force  $\dot{\mathbf{f}}_m \in \mathbb{R}^3$  and torque  $\dot{\boldsymbol{\tau}}_m \in \mathbb{R}^3$  that step the tip of the endoscope toward a desired heading,  $\hat{\mathbf{m}}_{c_{des}}$ . To compute infinitesimal wrench, we linearize the field in terms of EPM motion by utilizing the dipole-dipole model that has been shown to be accurate for cylindrical permanent magnets, especially as the distance between them increases [19]. Benefits of optimizing over end-effector motion are the ability to act on and constrain EPM motion directly as well as to weigh optimization contributions to favor linear or angular EPM motion. This is because, as seen in (2) and (3), magnetic force and torque are functions of both relative positions and orientations of both magnets, and thus, torque can be increased by either rotating the EPM or translating it in the proper direction. In this work, we regulate the height of the EPM so as to keep it constant throughout a retroflexion maneuver. The magnetic field of the EPM is expressed as:

$$\mathbf{B}_{EPM} = \frac{\mu_0 \|\mathbf{m}_a\|}{4\pi \|\mathbf{p}\|^3} D \hat{\mathbf{m}}_a \quad (1)$$

where  $D = 3\hat{\mathbf{p}}\hat{\mathbf{p}}^\top - I$ . The force,  $\mathbf{f}_m$ , and torque,  $\boldsymbol{\tau}_m$ , induced on the EM are expressed in vector form as:

$$\begin{aligned} \mathbf{f}_m(\mathbf{p}, \hat{\mathbf{m}}_a, \hat{\mathbf{m}}_c) &= (\mathbf{m}_c \cdot \nabla) \mathbf{B}_{EPM} \\ &= \frac{3\mu_0 \|\mathbf{m}_a\| \|\mathbf{m}_c\|}{4\pi \|\mathbf{p}\|^4} (\hat{\mathbf{m}}_a \hat{\mathbf{m}}_c^\top \\ &\quad + \hat{\mathbf{m}}_c \hat{\mathbf{m}}_a^\top + (\hat{\mathbf{m}}_c^\top Z \hat{\mathbf{m}}_a) I) \hat{\mathbf{p}} \end{aligned} \quad (2)$$

$$\begin{aligned} \boldsymbol{\tau}_m(\mathbf{p}, \hat{\mathbf{m}}_a, \hat{\mathbf{m}}_c) &= \mathbf{m}_c \times \mathbf{B}_{EPM} \\ &= \frac{\mu_0 \|\mathbf{m}_a\| \|\mathbf{m}_c\|}{4\pi \|\mathbf{p}\|^3} \hat{\mathbf{m}}_c \times D(\hat{\mathbf{p}}) \hat{\mathbf{m}}_a \end{aligned} \quad (3)$$

where  $Z = I - 5\hat{\mathbf{p}}\hat{\mathbf{p}}^\top$ . The relationship between the applied magnetic wrench and the EPM's pose is linearized analytically at each time step in the following manner:

$$\begin{aligned} \begin{bmatrix} \dot{\mathbf{f}}_m \\ \dot{\boldsymbol{\tau}}_m \end{bmatrix} &= \begin{bmatrix} \frac{\partial \mathbf{f}_m}{\partial \mathbf{p}_a} & \frac{\partial \mathbf{f}_m}{\partial \hat{\mathbf{m}}_a} \\ \frac{\partial \boldsymbol{\tau}_m}{\partial \mathbf{p}_a} & \frac{\partial \boldsymbol{\tau}_m}{\partial \hat{\mathbf{m}}_a} \end{bmatrix} \begin{bmatrix} I & 0 \\ 0 & S(\hat{\mathbf{m}}_a)^\top \end{bmatrix} \begin{bmatrix} \dot{\mathbf{p}}_a \\ \boldsymbol{\omega}_a \end{bmatrix} \\ &= J_{ft} \dot{\mathbf{x}}_a \end{aligned} \quad (4)$$

where  $S(\mathbf{a}) \in \mathfrak{so}(3)$  denotes the skew-symmetric form of the cross-product operation. Given the EM and EPM's discrete position, we optimize the linear and angular velocity of the EPM,  $\dot{\mathbf{x}}_a \in \mathbb{R}^6$ , such that an infinitesimal wrench magnitude reduces

heading error; we designate this heading-error-reducing direction by using the subscript "dir" in the objective function as follows:

$$\begin{aligned} \text{maximize}_{\dot{\mathbf{x}}_a} & \quad \left\| \begin{bmatrix} \dot{\mathbf{f}}^{m_{dir}} \\ \dot{\boldsymbol{\tau}}^{m_{dir}} \end{bmatrix} \right\|^2 \\ \text{subject to} & \quad \|W_c \dot{\mathbf{x}}_a\|^2 = \text{a constant} \end{aligned} \quad (5)$$

Here, the diagonal weight constraint matrix  $W_c \in \mathbb{R}^{6 \times 6}$  is used to specify how much the solution should favor more translation or rotation of the EPM. In our application, we are optimizing a vector that has two units: m/s for linear EPM velocity, and rad/s for angular EPM velocity. This unit mismatch has the same impact as the linear and angular components of a Jacobian being in disproportion. We use  $W_c$  to eliminate the effect of unit inequality by scaling up the linear weight.

By choosing an optimized  $\dot{\mathbf{x}}_a$  in the heading-error-reducing direction, we apply the maximum possible infinitesimal wrench that moves the tip such that heading error is reduced. To implement a direction preference in the objective function, we utilize a set of projection matrices in the optimization problem. If the force and torque Jacobians (linearizations of eq. 2 and eq. 3) were to be solely used to find  $\dot{\mathbf{x}}_a$ , the solution would result in an EPM motion that caused the maximum possible infinitesimal wrench without care for direction. To specify the favored directions in force and torque, we utilize projection matrix  $P_{ft} \in \mathbb{R}^{6 \times 6}$ , which results in the following formulation:

$$\begin{aligned} \begin{bmatrix} \dot{\mathbf{f}}^{m_{des}} \\ \dot{\boldsymbol{\tau}}^{m_{des}} \end{bmatrix} &= W_{ft} P_{ft} J_{ft} W_{EPM} \begin{bmatrix} \dot{\mathbf{p}}_a \\ \boldsymbol{\omega}_a \end{bmatrix} \\ &= J_{FT} \dot{\mathbf{x}}_a \end{aligned} \quad (6)$$

$P_{ft}$  is composed of three projection matrices:  $P_F$ ,  $P_T$ , and  $P_E$ , all  $\in \mathbb{R}^{3 \times 3}$ :

$$P_{ft} = \begin{bmatrix} P_F \\ P_E P_T \end{bmatrix} \quad (7)$$

$P_F$  is used to specify a desired direction of force application. We observe that applying a force in the direction of the desired heading assists in reducing the heading error. This is likely attributed to the effect of the body of the endoscope anchoring against the wall of the colon after its tip has retroflexed more than 90°. This projection is used only in the final 30° of the maneuver and is otherwise maintained as an identity matrix, thus the desired infinitesimal force is passively determined with proper torque application being favored. We define this projection matrix as  $P_F = \hat{\mathbf{m}}_{c_{des}} \hat{\mathbf{m}}_{c_{des}}^\top$ .

The infinitesimal torque direction is optimized under a few premises, to aid the explanation of which, we refer the reader to Fig. 3:

- 1) Owing to the symmetry of the EM, no torque can be applied in the direction along  $\hat{\mathbf{m}}_c$ ; thus the set of applicable torques must lie on plane  $P_{mc}$  as seen in Fig. 3.
- 2) A torque applied in the direction of  $\hat{\mathbf{m}}_{c_{des}}$  does not assist in reducing heading error; thus the plane orthogonal to  $\hat{\mathbf{m}}_{c_{des}}$ ,  $P_T$  in Fig. 3(a) and (c), is preferred for direction of torque application.

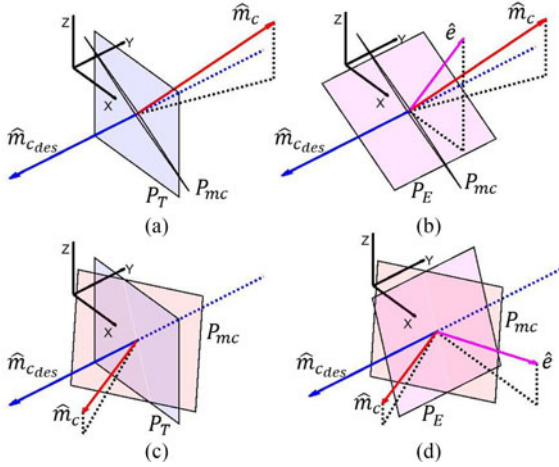


Fig. 3. Schematic visualization of the DoFs of magnetic torque application by the EPM onto the EM.  $P_{mc}$  shows the plane on which the actual applied torque lies and  $P_T$  and  $P_E$  are a visualization of the projection matrices used in our optimization technique. (a) and (b) show the effect of  $P_T$  and  $P_E$ , respectively, along with the applicable torque plane  $P_{mc}$  during the initial stage of retroflexion, while (c) and (d) show these concepts towards the end of retroflexion.

- 3) The ideal axis that reduces heading error is defined by  $\hat{\phi} = \hat{\mathbf{m}}_c \times \hat{\mathbf{m}}_{c_{des}}$ . An axis that is chosen to be orthogonal to  $\hat{\phi}$  can reduce heading error; however, cannot eliminate heading error completely if this axis is not continuously changed and is thus not preferred. We define this not-preferred axis as  $\hat{\mathbf{e}} = \hat{\mathbf{m}}_{c_{des}} \times \hat{\phi}$ . Rotation about  $\hat{\mathbf{e}}$ , because it is orthogonal to  $\hat{\mathbf{m}}_{c_{des}}$ , causes rotation away from the desired heading. We desire the torque axis to be orthogonal to  $\hat{\mathbf{e}}$  and thus on plane  $P_E$  as shown in Fig. 3(b) and (d).

We define projection matrices  $P_T = I - \hat{\mathbf{m}}_{c_{des}} \hat{\mathbf{m}}_{c_{des}}^\top$  and  $P_E = I - k_e \hat{\mathbf{e}} \hat{\mathbf{e}}^\top$  where  $k_e$  is a scalar that is used to weigh the effect of  $P_E$ . As aforementioned, we desire to find a solution  $\dot{\mathbf{x}}_a$  that imparts a maximum magnitude of infinitesimal torque onto the EM. This optimization process can be thought of as searching the plane of applicable torques,  $P_{mc}$ , and choosing  $\dot{\mathbf{x}}_a$  that imparts the largest projection of infinitesimal torque onto projection planes  $P_T$  and  $P_E$ . Fig. 3(a) and (b) show these projection planes at the beginning of the retroflexion, while Fig. 3(c) and (d) show these planes at the end of the retroflexion. During the beginning of retroflexion  $P_{mc}$  is closely aligned with  $P_T$ , therefore we prioritize the use of  $P_T$  by setting  $k_e$  to 0, which is maintained until the midpoint (90°) of the retroflexion. We note that from the beginning to this midpoint,  $P_T$  increasingly favors the infinitesimal torque to align with  $\hat{\phi}$  owing to the projection plane  $P_T$  becoming orthogonal to  $P_{mc}$ . On the contrary, as the tip of the endoscope is rotated from the midpoint to the desired heading, the opposite occurs and  $\hat{\phi}$  is favored less and less. When this happens, the algorithm does not punish the torque axis having a large component along  $\hat{\mathbf{e}}$ , which has the adverse effect of increasing heading error. To compensate for this effect, we scale up the effect of  $P_E$  by increasing  $k_e$  linearly from 0 at the midpoint of retroflexion to 1 as the endoscope becomes aligned with the desired heading. The symmetry of the

EM inherently limits us to 2 DoF in torque, i.e. vectors on  $P_{mc}$  plane in Fig. 3, and  $P_T$  and  $P_E$  do not eliminate a full DoFs but rather assist in specifying preferred directions of torque.

The diagonal weight matrices  $W_{EPM} \in \mathbb{R}^{6 \times 6}$  and  $W_{ft} \in \mathbb{R}^{6 \times 6}$ , seen in Eq. 6, are used for both designating preferred DoFs to act on, or completely constraining the solution.  $W_{EPM}$  can be used to punish unwanted EPM motion by setting corresponding weights between 0 and 1. Setting a diagonal element of  $W_{EPM}$  to 0 results in the respective EPM velocity DoF not influencing the resulting infinitesimal wrench, while setting a diagonal element of  $W_{ft}$  to 0 results in the respective infinitesimal wrench being 0. To demonstrate how such weights can be used, in our application we choose to set the third through sixth diagonal elements of  $W_{EPM}$  as functions of the angle between the world vertical axis and the manipulator's last link. This is a simple method to prevent contact of other robot links with the patient.  $W_{ft}$  allows for discriminating force and torque effects that dictate which components of the magnetic wrench to optimize. In other words, one can specify whether a higher torque or force application is preferred in a certain direction over another, an example of which is the desired avoidance of lateral force on the colon.

In the interest of real-time computation, we optimize via Lagrange multipliers with the following Lagrange function:

$$\mathcal{L}(\dot{\mathbf{x}}_a, \lambda) = \left\| \begin{bmatrix} \dot{\mathbf{f}}_{dir} \\ \dot{\boldsymbol{\tau}}_{dir} \end{bmatrix} \right\|^2 - \lambda \|W_c \dot{\mathbf{x}}_a\|^2 \quad (8)$$

We evaluate by standard means of setting a scaled gradient equality:

$$\nabla_{\dot{\mathbf{x}}_a} \left( \left\| \begin{bmatrix} \dot{\mathbf{f}}_{dir} \\ \dot{\boldsymbol{\tau}}_{dir} \end{bmatrix} \right\|^2 \right) = \lambda \nabla_{\dot{\mathbf{x}}_a} \|W_c \dot{\mathbf{x}}_a\|^2 \quad (9)$$

that is equivalent to:

$$J_{FT}^\top J_{FT} \dot{\mathbf{x}}_a = \lambda W_c^\top W_c \dot{\mathbf{x}}_a \quad (10)$$

and can be rapidly computed as an eigenvalue problem:

$$(W_c^\top W_c)^{-1} J_{FT}^\top J_{FT} \dot{\mathbf{x}}_a = A \dot{\mathbf{x}}_a = \lambda \dot{\mathbf{x}}_a \quad (11)$$

where  $A$  is  $\in \mathbb{R}^{6 \times 6}$  and the optimal vector  $\dot{\mathbf{x}}_a^*$  is the eigenvector that imparts an EPM motion that, in turn, applies the largest change in force and torque in the desired direction. Using gradient projection methods as introduced by [20], a redundant DoF resulting from the symmetry of cylindrical magnets is utilized for favorable link orientation with respect to the patient's general location. These joint rates acting in the EPM's linearized nullspace are referred to as  $\dot{\mathbf{q}}_R$ . Finally, the commands are converted into desired joint velocities by using the right pseudo-inverse of the manipulator's Jacobian, denoted by  $J_R^+ = J_R^\top (J_R J_R^\top)^{-1}$ , that produces a minimum joint norm solution which is coupled with the nullspace solution and sent to the robot.

$$\dot{\mathbf{q}} = J_R^+ \dot{\mathbf{x}}_a^* + \dot{\mathbf{q}}_R \quad (12)$$

## B. Reasoning Behind Chosen Optimal Solutions

As mentioned above,  $\hat{\phi}$  is the ideal axis for reducing heading error and if there was a rigid link between the EPM and EM

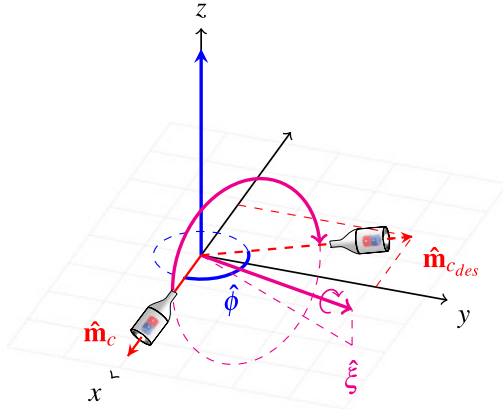


Fig. 4. The axis that defines the shortest angular path between current and desired heading  $\hat{\phi}$  vs. the maximum theoretical torque application axis  $\hat{\xi}$ . This schematic demonstrates that the two axes are not necessarily aligned.

then this axis should always be used to reduce heading error. However, owing to the nature of the dipole field, consideration must be made as to what is the best way to apply a magnetic torque between dipoles. Past works, such as [13], [15], [18], set desired infinitesimal torque directions about  $\hat{\phi}$ ; however, we now demonstrate that this is typically not the most effective axis to apply torque about. We show that one must take into account the relative poses of the magnetic fields when determining how a heading error should be minimized.

We define an ideal torque application axis,  $\hat{\xi}$ , about which the greatest possible torque can be applied on the actuated magnet and is a function of the relative magnet poses. A schematic describing the concept is shown in Fig. 4. Let us first examine a simple case where the magnet heading is along the world  $x$  axis,  $\hat{\mathbf{m}}_c = [1, 0, 0]^T$ , the EPM heading is along the world  $-x$  axis  $\hat{\mathbf{m}}_a = [-1, 0, 0]^T$ , and the EM is located directly under the EPM ( $\hat{\mathbf{p}} = [0, 0, -1]^T$ ). This is a typical initial configuration for retroflexion, and an axis of rotation must be decided. Rotation about the  $x$  axis is fruitless owing to axial symmetry of the magnets, and we are left with either a  $y$  or  $z$  rotation, or a combination of the two. We are interested in which rotation has the largest magnitude of  $\delta\tau_m$  which is defined as follows [13]:

$$\begin{aligned} \delta\tau_m &= \frac{\mu_0 \|\mathbf{m}_a\| \|\mathbf{m}_c\|}{4\pi \|\mathbf{p}\|^3} S(\hat{\mathbf{m}}_c)(3\hat{\mathbf{p}}\hat{\mathbf{p}}^T - I)\delta\mathbf{m}_a \\ &= C(3\hat{\mathbf{m}}_c \times \hat{\mathbf{p}}\hat{\mathbf{p}}^T \delta\mathbf{m}_a) - C(\hat{\mathbf{m}}_c \times \delta\hat{\mathbf{m}}_a) \end{aligned} \quad (13)$$

where  $C$  is a constant and the first term considers the projected component of  $\delta\hat{\mathbf{m}}_a$  onto the relative position axis that is normal to the heading of the endoscope, while the second is independent of position. If  $\delta\hat{\mathbf{m}}_a = [0, 0, 1]$  then  $\delta\tau_m = [0, -2, 0]$ , while if  $\delta\hat{\mathbf{m}}_a = [0, 1, 0]$ , then  $\delta\tau_m = [0, 0, -1]$  and thus we see more efficiency in the vertical ( $z$ ) increase in  $\hat{\mathbf{m}}_a$ . The two-factor magnitude increase of  $\delta\tau_m$  occurred here owing to orthogonality of  $\delta\hat{\mathbf{m}}_a$  and  $\hat{\mathbf{p}}$ , however, this magnitude will typically scale with the cosine of the angle between them. Seeing that varying the axis of rotation can impact torque magnitude as much as two-fold, it is reasonable to assume that the best axis of rotation is not necessarily the one that defines the shortest path between

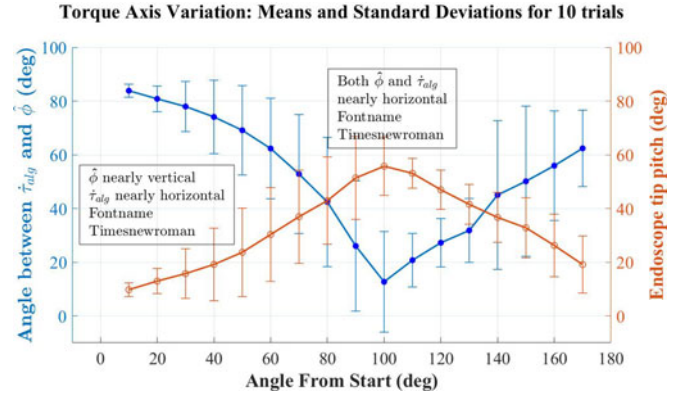


Fig. 5. A piecewise linear representation of the means and standard deviations of 10 retroflexion trials showing the difference between the shortest path axis and the chosen optimal rotation axis, where of interest is the general shapes of the curves. Note that the high variance between data sets is acceptable and is attributed to the trials being independent of each other, which is expected owing to the system responding to the motion of the endoscope rather than following a preplanned trajectory.

the current and desired heading. A trade-off will then exist between the magnitude and directness of each possible torque axis. Owing to our necessity for high torque to overcome the endoscope body's bending stiffness and to move through a tortuous and deformable colon environment, we allow the algorithm to always choose the highest torque inducing motion for the end effector.

To demonstrate that our algorithm chooses axes other than  $\hat{\phi}$ , we recorded the algorithm's chosen infinitesimal axis,  $\hat{\tau}_{alg}$ , of torque application (note that in previous works this was chosen to be  $\hat{\tau}_{alg} = \hat{\phi}$ ). As seen in Fig. 5, there exists a visible variance between each trial; however, this is expected as each retroflexion trial is dependent on the current behavior of the endoscope, thus trials should not be expected to have identical behavior. Data is plotted as a function of the angle between  $\hat{\mathbf{m}}_c$  and  $\hat{\mathbf{m}}_{c_{des}}$ . As the maneuver starts, there is over an  $80^\circ$  difference between  $\hat{\phi}$  and  $\hat{\tau}_{alg}$ . This difference is attributed to  $\hat{\phi}$  being nearly vertical (because of  $\hat{\mathbf{m}}_c$  being nearly horizontal) while  $\hat{\tau}_{alg}$  is nearly horizontal. As the pitch of the tip increases ( $\hat{\mathbf{m}}_c$  approaches a vertical heading), the difference between  $\hat{\phi}$  and  $\hat{\tau}_{alg}$  reduces significantly. When choosing the axis of infinitesimal torque, we must compromise between choosing the axis of maximum torque application and an axis that reduces the heading error.

## IV. VALIDATION

### A. Validating Retroflexion

To evaluate the algorithm, a series of bench-top trials were conducted on the platform shown in Fig. 1. Of utmost importance in setting experimental parameters was clinical relevance. Plastic tube sizes of 38 mm, 44 mm, 50 mm, and 60 mm were chosen as they fall in the range of adult human colon diameters: 20-120 mm, where a 120 mm diameter can be reached at the apex of the sigmoid colon [21], [22]. Setting the desired height of the EPM necessitates the consideration of both patient location and the decay of field strength with distance. We specify a virtual barrier, which we call the "no-cross height", as the

TABLE I  
EXPERIMENTAL RESULTS

Tube I.D. (mm)	No-Cross Height (mm)	Mean Time (s)	Std. Dev. (s)	No. Successes out of 10 Trials	Mean Force (N)	Mean Torque (Nm)
60	40	10.5	0.6	10	0.741	0.0111
	50	17.0	10.8	10	0.518	0.0113
	60	15.9	2.8	6	0.403	0.0112
50	40	12.0	0.5	10	0.615	0.0116
	50	14.4	0.9	10	0.465	0.0112
	60	15.9	0.9	2	0.375	0.0107
44	40	11.6	1.4	10	0.663	0.0130
	50	13.3	0.5	9	0.505	0.0129
	60	N/A	N/A	0	N/A	N/A
38	40	14.6	0.5	10	0.591	0.0153
	50	19.3	5.3	10	0.439	0.0151
	60	27.3	5.2	4	0.326	0.0149
Ex-vivo (47)	50	19.7	2.9	10	0.538	0.0193

vertical distance above the colon wall that cannot be crossed by the EPM. Owing to the adult male’s mid-sagittal abdominal wall thickness being 15–20 mm [23] and an approximate colon tissue thickness of 1 mm [24], we chose the no-cross height to be 40 mm, 50 mm, and 60 mm for experiments, giving at least nearly 20 mm of leeway for a layer of fat at the worst case. An increase in magnet strength can easily allow for a larger spacing. For each combination of tube diameter and no-cross height, 10 trials were conducted with results shown in Table I. For a trial to be labeled as successful, the endoscope’s heading had to reach within  $10^\circ$  of the desired retroflexed heading. The algorithm completion success rate was 98.8% for EPM spacings of 50 mm and below; however, this success rate drastically dropped when the spacing was increased to 60 mm owing to an inability to impart a sufficient magnetic wrench.

To verify the clinical applicability of the method, a set of 10 trials was conducted on a freshly-excised porcine colon, which is anatomically similar to that of a human [25]. The colon was mounted inside a 47 mm inner diameter tube—the mean diameter of the human colon [22]—as shown in Fig. 6. We note that the tissue appears to fully expand into the diameter of the tube, and thus approximate the inner diameter of the colon to be that of the tube, or 47 mm. As seen in the last row of Table I, a 100% success rate was achieved with a mean maneuver duration of 19.7 s. This is approximately 1.6% of the average duration of adult colonoscopy with no intervention ( $21.1 \pm 10.4$  min [26]). During one of the trials inside the 60 mm ID tube at a no-cross height of 50 mm, the endoscope slipped and the external magnet was forced to make motions that were out of the ordinary to eventually achieve a successful retroflexion. This caused a trial time of 47.5 s and thus raised the mean trial time to  $17.0 \pm 10.8$  s. Without this outlier, the mean retroflex time for trials inside the 60 mm ID tube at a no-cross height of 50 mm was 13.6 s. The outlier was not omitted as the algorithm did succeed in overcoming the unexpected difficulty. Additionally, we note that as the no-cross height is lower, a greater magnetic force and torque are applied by the EPM onto the magnet, and thus trials with a lower no-cross height tend to have a shorter time of retroflexion, which can be seen in Table I. The mean

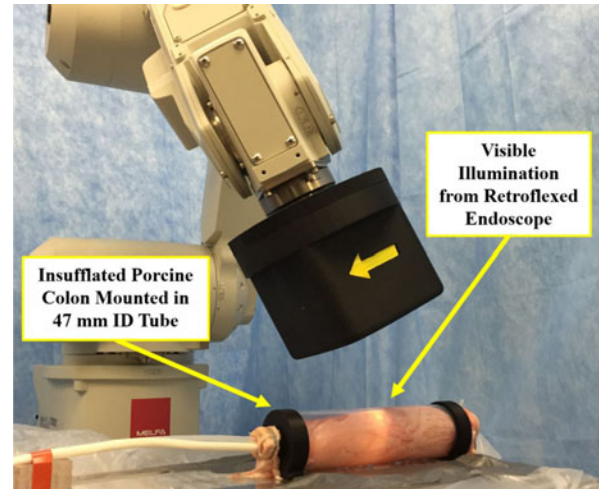


Fig. 6. Photo of ex vivo trial setup. A set of 10 trials was conducted using porcine colon tissue.

time of retroflexion during the *ex vivo* trial was approximately 5 s slower than that of trials conducted in plastic tubes with similar inner diameters (44 mm and 50 mm) with the same EPM spacing. This longer time of retroflexion inside real tissue is likely attributed to the added resistance of tissue deformation as well as the tissue stretching that is not typically encountered *in vivo* owing to the presence of the mesentery (i.e., tissue that connects organs to the body). Footage of both in-tube trials as well as the *ex vivo* assessment can be seen in the multimedia attachment.

### B. Tissue Stress Measurement

While applying proper forces and torques to achieve retroflexion may be achievable, it is necessary that the resulting reaction on tissue does not induce damage. The applied magnetic force and torque on the EM can be monitored and bounded [27]; however, an additional reaction on tissue—resulting from the bending stiffness of the body of the endoscope applying a moment on the EM—occurs and is present after the tip of the endoscope passes the half-way point of the retroflexion. To experimentally measure the force applied by the endoscope on the colon wall, an experimental setup, seen in Fig. 7(a), was designed. A 60 mm ID tube was cut along its length such that the endoscope made contact with one side that was rigidly coupled with a 6-axis force/torque sensor (Nano 17 SI-25-0.25, ATI Technologies Inc., Canada) while the body of the endoscope made contact with the other.

As shown in the schematic in Fig. 7(b), the body of the endoscope exerts a negligible distributed load on the (what is shown as) bottom tissue wall and is thus ignored. On the other hand, the endoscope applies on the top wall a combination of magnetic force, reaction force from the endoscope body’s bending stiffness, and forces from friction and tissue deformation. Although effects of tissue deformation are not considered here, they have been investigated in [28]. Note that the aforementioned negligible distributed load and the reaction force on the endoscope from the endoscope body’s bending are similar in magnitude; how-

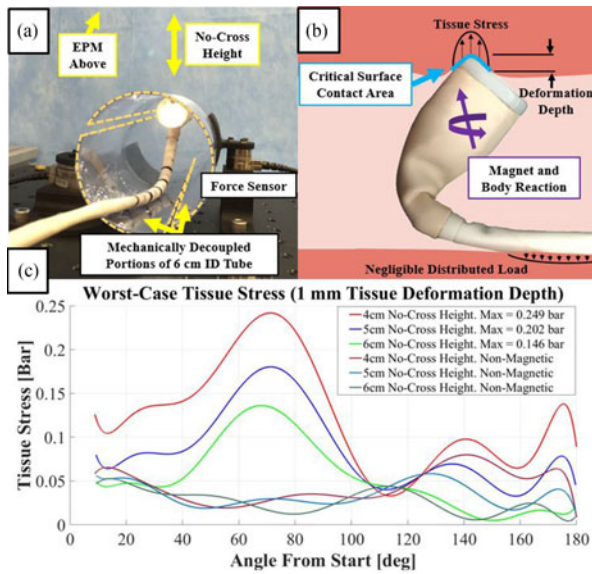


Fig. 7. a) Setup for force sensing during a retroflex. b) Schematic diagram of the distributed load of the body of the endoscope as well as the stress concentration at the contact point between the tip of the endoscope and colonic tissue. c) Best fit curves of stress computed from force measured through 3 sets of 10 trials and the contact area as computed at the tip of the endoscope, shown in (b).

ever, the loads are distributed differently. The measured force is projected onto the normal direction to the tube at the point of contact with the tip of the endoscope, which is known owing to real-time localization. Of importance is resultant tissue stress, rather than force.

To make a worst-case stress approximation, we assume the endoscope to be oriented such that a minimum surface area is making contact with tissue, as shown in Fig. 7(b). We make an assumption that the tip of the endoscope “digs” into the tissue by 1 mm, giving a 1 mm deformation depth. Knowing the geometry of the tip of the endoscope, this “critical area” can be trivially computed and is used in any stress computation henceforth. This critical area is outlined in blue in Fig. 7(b). Three sets of 10 retroflexion trials at various no-cross heights were conducted inside this sensing tube with best fit curves shown for clarity in Fig. 7(c). Additionally, for each of these sets, we subtracted the magnetic force that was computed via dipole-dipole model to obtain the non-magnetic force profile. This profile, largely dependant on the endoscope body’s stiffness as suggested by the increase in non-magnetic force after a  $90^\circ$  angle from start of the maneuver, is represented with best fit curves in Fig. 7(c). It is noteworthy that this body stress is significantly lower than the magnetic force, thus monitoring and throttling magnetic force may be sufficient for safe manipulation of the device. As seen in Fig. 7(c), the maximum applied tissue stress is 0.249 bar, which is only 8.3% of the 3 bar stress that may induce tissue damage [29].

## V. CONCLUSION

In this work, we developed an algorithm for the autonomous retroflexion of a magnetic flexible endoscope. Using a real-time force and torque magnitude optimization, the system chooses

an instantaneous wrench to impart on the EM that results in the most effective motion towards its desired (retroflexed) heading. We validated the approach by demonstrating retroflexion of the tip of the endoscope with a 98.8% success rate in plastic tubes of various sizes while the EPM’s no-cross height was within 50 mm of the colon. Additionally, we demonstrated retroflexion of the endoscope on an insufflated porcine colon of inner diameter similar to that of the average human colon diameter (47 mm). The set of 10 *ex vivo* trials resulted in a 100% success rate in a mean maneuver time of  $19.7 \pm 2.9$  s. Although a larger magnetic field source can always be pursued, our aim was to use a permanent magnet that could be carried by a serial manipulator and make the most effective motions possible with it to accomplish the task at hand. Given that retroflexing an endoscope may require significant forces and torques, we developed a platform to measure applied normal force, and, in turn, approximate the maximum applied tissue stress. Using a worst-case tissue contact area approximation, the maximum applied tissue stress was determined to be 91.7% below what is necessary to damage tissue.

An additional contribution of this work is our consideration for the efficiency of a rotation axis of the endoscope; a concept that applies to any magnetic device. While magnetic controllers in the past have acted on an error defined by the cross product of current and desired device heading, we have shown that this is typically not the ideal rotation axis. As we demonstrate in this letter, the non-intuitive interaction between dipole fields causes significant misalignment between the two axes. How much torque can be applied for a given magnet configuration and desired heading must be considered when choosing a rotation axis for a magnetic device (the tip of the endoscope in our case). Therefore, an efficiency measure should be used to compromise between rotation distance and an ability to apply torque. In future works involving magnetic manipulation, this concept can be extended such that the need for optimization, as done in this letter, is eliminated, and rotation axes are chosen with a foreseeable rotational efficiency measure.

In summary, our autonomous platform for retroflexing a magnetically actuated colonoscope is a robust, fast, and safe technique that may improve the quality of colonoscopy and reduce colon cancer.

## ACKNOWLEDGMENT

We would like to thank Medical Murray, IL, USA for assistance with fabrication of the flexible endoscope. Any opinions, findings, conclusions, or recommendations expressed in this material are those of the authors and do not necessarily reflect the views of the National Institutes of Health, the National Science Foundation, or the Royal Society.

## REFERENCES

- [1] A. Jemal, F. Bray, M. M. Center, J. Ferlay, E. Ward, and D. Forman, “Global cancer statistics,” *CA, Cancer J. Clinicians*, vol. 61, no. 2, pp. 69–90, 2011.
- [2] M. F. Kaminski *et al.*, “Quality indicators for colonoscopy and the risk of interval cancer,” *New England J. Med.*, vol. 362, no. 19, pp. 1795–1803, 2010.

- [3] M. Rubin, L. Lurie, K. Bose, and S. H. Kim, "Expanding the view of a standard colonoscope with the third eye panoramic cap," *World J. Gastroenterology*, vol. 21, no. 37, 2015, Art. no. 10683.
- [4] S. Chandran *et al.*, "Right-sided adenoma detection with retroflexion versus forward-view colonoscopy," *Gastrointestinal Endoscopy*, vol. 81, no. 3, pp. 608–613, 2015.
- [5] R. E. Sedlack *et al.*, "Colonoscopy core curriculum," *Gastrointestinal Endoscopy*, vol. 76, no. 3, pp. 482–490, 2012.
- [6] A. M. Leufkens *et al.*, "Effect of a retrograde-viewing device on adenoma detection rate during colonoscopy: The terrace study," *Gastrointestinal Endoscopy*, vol. 73, no. 3, pp. 480–489, 2011.
- [7] P. Valdastrì, M. Simi, and R. J. Webster III, "Advanced technologies for gastrointestinal endoscopy," *Annu. Rev. Biomed. Eng.*, vol. 14, pp. 397–429, 2012.
- [8] P. R. Slawinski, K. L. Obstein, and P. Valdastrì, "Emerging issues and future developments in capsule endoscopy," *Techn. Gastrointestinal Endoscopy*, vol. 17, no. 1, pp. 40–46, 2015.
- [9] L. J. Sliker and G. Ciuti, "Flexible and capsule endoscopy for screening, diagnosis, and treatment," *Expert Rev. Med. Devices*, vol. 11, no. 6, pp. 649–666, 2014.
- [10] P. Valdastrì *et al.*, "Magnetic air capsule robotic system: Proof of concept of a novel approach for painless colonoscopy," *Surg. Endoscopy*, vol. 26, no. 5, pp. 1238–1246, 2012.
- [11] G. D. Hager, D. Rus, V. Kumar, and H. Christensen, "Toward a science of autonomy for physical systems," arXiv preprint arXiv:1604.02979, 2016.
- [12] C. Di Natali, M. Beccani, and P. Valdastrì, "Real-time pose detection for magnetic medical devices," *IEEE Trans. Magn.*, vol. 49, no. 7, pp. 3524–3527, Jul. 2013.
- [13] A. Z. Taddese, P. R. Slawinski, K. L. Obstein, and P. Valdastrì, "Closed loop control of a tethered magnetic capsule endoscope," in *Proc. 2016 Robot., Sci. Syst.*, Ann Arbor, Michigan, USA, 2016, pp. 1–9.
- [14] C. Di Natali, M. Beccani, N. Simaan, and P. Valdastrì, "Jacobian-based iterative method for magnetic localization in robotic capsule endoscopy," *IEEE Trans. Robot.*, vol. 32, no. 2, pp. 327–338, Apr. 2016.
- [15] A. Z. Taddese, P. R. Slawinski, K. L. Obstein, and P. Valdastrì, "Non-holonomic closed-loop velocity control of a soft-tethered magnetic endoscope," in *Proc. IEEE/RSJ Int. Conf. Intell. Robot. Syst.*, Daejeon, South Korea, 2016, pp. 1139–1144.
- [16] T. D. Than *et al.*, "An effective localization method for robotic endoscopic capsules using multiple positron emission markers," *IEEE Trans. Robot.*, vol. 30, no. 5, pp. 1174–1186, Oct. 2014.
- [17] K. M. Popek and J. J. Abbott, "6-D localization of a magnetic capsule endoscope using a stationary rotating magnetic dipole field," in *Proc. Hamlyn Symp. Med. Robot.*, 2015, pp. 47–48.
- [18] A. W. Mahoney and J. J. Abbott, "Five-degree-of-freedom manipulation of an untethered magnetic device in fluid using a single permanent magnet with application in stomach capsule endoscopy," *Int. J. Robot. Res.*, vol. 35, pp. 129–147, 2016.
- [19] A. J. Petruska and J. J. Abbott, "Optimal permanent-magnet geometries for dipole field approximation," *IEEE Trans. Magn.*, vol. 49, no. 2, pp. 811–819, Feb. 2013.
- [20] A. Liegeois, "Automatic supervisory control of the configuration and behavior of multibody mechanisms," *IEEE Trans. Syst., Man, Cybern.*, vol. SMC-7, no. 12, pp. 868–871, Dec. 1977.
- [21] B. Bhatnagar, C. Sharma, S. Gupta, M. Mathur, and D. Reddy, "Study on the anatomical dimensions of the human sigmoid colon," *Clinical Anatomy*, vol. 17, no. 3, pp. 236–243, 2004.
- [22] A. Alazmani, A. Hood, D. Jayne, A. Neville, and P. Culmer, "Quantitative assessment of colorectal morphology: Implications for robotic colonoscopy," *Med. Eng. Phys.*, vol. 38, no. 2, pp. 148–154, 2016.
- [23] G. Sandler, S. Leishman, H. Branson, C. Buchan, and A. J. Holland, "Body wall thickness in adults and children—relevance to penetrating trauma," *Injury*, vol. 41, no. 5, pp. 506–509, 2010.
- [24] V. I. Egorov, I. V. Schastlivtsev, E. V. Prut, A. O. Baranov, and R. A. Turusov, "Mechanical properties of the human gastrointestinal tract," *J. Biomech.*, vol. 35, no. 10, pp. 1417–1425, 2002.
- [25] H. Hoeg, A. B. Slatkin, J. W. Burdick, and W. S. Grundfest, "Biomechanical modeling of the small intestine as required for the design and operation of a robotic endoscope," in *Proc. IEEE Int. Conf. Robot. Autom.*, 2000, vol. 2, pp. 1599–1606.
- [26] R. E. Childers, J. L. Williams, and A. Sonnenberg, "Practice patterns of sedation for colonoscopy," *Gastrointestinal Endoscopy*, vol. 82, no. 3, pp. 503–511, 2015.
- [27] C. Di Natali, M. Beccani, K. L. Obstein, and P. Valdastrì, "A wireless platform for in vivo measurement of resistance properties of the gastrointestinal tract," *Physiological Meas.*, vol. 35, no. 7, pp. 1197–1214, 2014.
- [28] L. J. Sliker, G. Ciuti, M. E. Rentschler, and A. Menciassi, "Frictional resistance model for tissue-capsule endoscope sliding contact in the gastrointestinal tract," *Tribology Int.*, vol. 102, pp. 472–484, 2016.
- [29] M. Moshkowitz *et al.*, "A novel device for rapid cleaning of poorly prepared colons," *Endoscopy*, vol. 42, no. 10, pp. 834–836, 2010.